Dynamics of Two Parallel Inverted Flags in Axial Flow

Shaoguang Wang, Mathias Legrand, Michael Païdoussis

Dynamics of Two Parallel Inverted Flags in Axial Flow

Shaoguang Wang, Mathias Legrand, Michael Païdoussis

Department of Mechanical Engineering, McGill University, Montreal, Quebec, Canada

ABSTRACT

Two identical thin flexible plates, referred to as "inverted flags", in a side-by-side arrangement are investigated theoretically. A linear model is developed to predict the onset of instability. This linear model elucidates the mechanism of instability and the sensitivity of the critical flow velocity to the gap between the two flags. The dynamics of a single flag has been studied massively, but the coupling of multiple flags is seldom reported. The Euler-Bernoulli beam theory and incompressible potential flow theory are adopted in the model. The Galerkin method and Fourier transform technique are used to solve flag displacements and fluid potentials, respectively. As the flow velocity is increased, the first mode becomes unstable via a pitchfork bifurcation. At higher flow velocities, higher modes lose stability via Hopf bifurcations. Out-of-phase and in-phase motions are predicted for the two flags. It is found that the critical velocity is independent of the flag gap-to-length ratio when it is approximately greater than 1. When the ratio is reduced, the critical velocity becomes smaller. When the ratio is extremely small, flutter occurs to the first mode before static divergence.

Keywords: Inverted flags, linear stability analysis

1. INTRODUCTION

Recently, inverted flags have been of great interest in energy harvesting systems due to large-amplitude flapping they might feature and large strain energy they can store [1, 2]. An underwater energy harvester can start up at extremely low ocean current speeds and have a wide working range [3]. Flapping motions are also considered in order to enhance the performance of some types of heat exchangers [4]. A flag-fluid model was even used to study human snoring [5].

The dynamics of a single inverted flag has been vigorously investigated theoretically and experimentally. The aspect and mass ratios are commonly the most important parameters. It has been found that, for a slender flag, a larger mass ratio has the effect of generating instability at lower flow velocities, while for a two-dimensional flag, the mass ratio has no impact on the critical point for static divergence, but it does for the onset of flutter [6, 7]. The underlying mechanism giving rise to flapping initially considered to be a vortex-induced vibration (VIV) [8, 9] was shown to be self-excited [10]. Particularly for heavy flags, periodic vortex shedding is not the cause but a consequence of large-amplitude flapping.

The purpose of this study is to develop a mathematical model that predicts the instabilities of two parallel inverted flags in axial airflow, as in Fig. 1. It is assumed that both flags undergo one-dimensional motions and the fluid satisfies a two-dimensional potential flow assumption. The Galerkin method is employed to solve the equations of motion, and the Fourier transform technique is adopted to obtain the perturbation pressure in terms of flag displacements.

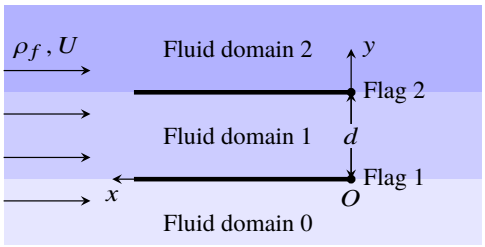

FIGURE 1: TWO PARALLEL INVERTED FLAGS IN AXIAL FLOW

2. GOVERNING EQUATIONS AND BOUNDARY CONDITIONS

The equation governing the dynamics of the transverse displacement $w^{(j)}(x,t)$ of flag j ($j = 1, 2$) reads

$$\rho_p h_p \partial_t^2 w^{(j)} + D\partial_x^4 w^{(j)} + p^{(j)} = 0 \tag{1}$$

where ρ_p is the flag density, h_p, the flag thickness, function of space x and time t, $D = Eh_p^3/[12(1-\nu^2)]$, the flag stiffness, E, Young's modulus, ν, Poisson's ratio, and $p^{(j)}(x,t)$, the perturbation pressure acting on flag j. The notation $\partial_x u$ means partial derivative of the quantity u with respect to argument x. The boundary conditions are given by

$$\begin{aligned} &w^{(j)}(0,t) = \partial_x w^{(j)}(0,t) = \partial_x^2 w^{(j)}(L,t) = 0, \\ &D\partial_x^3 w^{(j)}(L,t) = \rho_f LU(\partial_t w^{(j)}(L,t) - U\partial_x w^{(j)}(L,t)) \end{aligned} \tag{2}$$

where L is the flag length, ρ_f, the fluid density, and U, the free flow velocity. Incorporating the shear force boundary condition into Eq. (1) by means of a Dirac delta function yields

$$\begin{aligned} \rho_p h_p \partial_t^2 w^{(j)} + D\partial_x^4 w^{(j)} + p^{(j)} \\ + \rho_f LU(\partial_t w^{(j)} - U\partial_x w^{(j)})\delta(x-L) = 0. \end{aligned} \tag{3}$$

The reason for doing this is that the system can be analyzed with the flag treated as a standard cantilever beam subject to the simple free-clamped boundary conditions [11].

The perturbation potential $\Phi^{(n)}(x,y,t)$ in fluid domain n ($n = 0, 1, 2$) satisfies the Laplace equation

$$\partial_x^2 \Phi^{(n)} + \partial_y^2 \Phi^{(n)} = 0 \tag{4}$$

along with the boundary conditions

$$\begin{aligned} \partial_y \Phi^{(j-1)}(x,(j-1)d,t) &= \partial_y \Phi^{(j)}(x,(j-1)d,t) \\ &= (\partial_t - U\partial_x) w^{(j)}(x,(j-1)d,t), \quad j = 1,2 \\ \partial_y \Phi^{(0)}(x,-\infty,t) &= \partial_y \Phi^{(2)}(x,+\infty,t) = 0 \end{aligned} \tag{5}$$

where d is the gap between the two flags.

The perturbation pressure $p^{(j)}(x,t)$ on flag j is given by the linearized unsteady Bernoulli equation

$$p^{(j)} = -\rho_f(\partial_t - U\partial_x)[\Phi^{(j)} - \Phi^{(j-1)}] \text{ at } (x,(j-1)d,t). \quad (6)$$

Elsewhere the perturbation pressure is zero, i.e. $p = 0$ for $x < 0$ and $x > L$.

To make these equations dimensionless and analyze the problem in the frequency domain, we define the following dimensionless quantities with asterisks: $x = x^*L$, $y = y^*L$, $d = d^*L$, $\mu = \rho_f L/(\rho_p h_p)$, $t = t^*L^2\sqrt{\rho_p h_p/D}$, $\Omega = \sqrt{D}\omega^*/(L^2\sqrt{\rho_p h_p}$, $U = U^*\sqrt{D}/(L\sqrt{\rho_p h_p})$, $w(x,t) = w^*(x^*)Le^{i\Omega t}$, $p(x,t) = p^*(x^*)e^{i\Omega t}D/L^3$, and $\Phi(x,y,t) = \phi^*(x^*,y^*)e^{i\Omega t}\sqrt{D}/\sqrt{\rho_p h_p}$. Substituting into Eqs. (3), (4) and (6) and dropping the asterisks for simplicity (valid in the following sections as well), the dimensionless governing equations are

$$w''''^{(j)} - \omega^2 w^{(j)} + p^{(j)} + \mu U(i\omega w^{(j)} - U w'^{(j)})\delta(x-1) = 0 \quad (7a)$$

$$\partial_x^2\phi^{(n)} + \partial_y^2\phi^{(n)} = 0 \quad (7b)$$

$$p^{(j)} = -\mu(i\omega - U\partial_x)[\phi^{(j)} - \phi^{(j-1)}]\big|_{(x,(j-1)d)}. \quad (7c)$$

The prime notation $u'(x)$ means first derivative of the function u with respect to variable x; u'', the second derivative, and so on. The dimensionless boundary conditions for flag displacements and fluid potentials are

$$w^{(j)}(0) = w'^{(j)}(0) = w''^{(j)}(1) = w'''^{(j)}(1) = 0 \quad (8)$$

and

$$\begin{aligned} &\partial_y\phi^{(j-1)} = \partial_y\phi^{(j)} = i\omega w^{(j)} - U w'^{(j)} \text{ at } (x,(j-1)d) \\ &\partial_y\phi^{(0)}(x,-\infty) = \partial_y\phi^{(2)}(x,+\infty) = 0. \end{aligned} \quad (9)$$

3. SOLUTION METHODS

The Galerkin method is used to solve the equation of motion (7a). The displacement of each flag is decomposed using the first Q eigenfunctions of a cantilever beam in vacuum

$$w^{(j)}(x) = \sum_{n=1}^{Q} A_n^{(j)}\psi_n(x). \quad (10)$$

Since the perturbation pressures on the flags are unknown, the relation between pressures and displacements must be determined first.

3.1 Perturbation pressures

Following the work on two parallel conventional (i.e., clamped-free) flags by Michelin and Llewellyn Smith [12], the derivation of the perturbation pressure is briefly summarized here. Interested readers can refer to [12–14]. Note that the difference for inverted flags is that the flow direction is reversed, i.e. there is a sign difference in the flow velocity. The Laplace equation (7b) is solved using the Fourier transform with respect to x, and a general solution is obtained with coefficients to be determined by the boundary conditions (9). Using the Bernoulli equation (7c), the perturbation pressure can be expressed in terms of the flag displacement as follows:

$$\begin{aligned} &\frac{1}{2\pi\mu}\left(\int_0^1 \frac{p'^{(1)}(\xi)}{x-\xi}d\xi + \int_0^1 \frac{x-\xi}{(x-\xi)^2+d^2}p'^{(2)}(\xi)d\xi\right) \\ &\quad = -\omega^2 w^{(1)}(x) - 2i\omega U w'^{(1)}(x) + U^2 w''^{(1)}(x) \end{aligned} \quad (11a)$$

and

$$\begin{aligned} &\frac{1}{2\pi\mu}\left(\int_0^1 \frac{p'^{(2)}(\xi)}{x-\xi}d\xi + \int_0^1 \frac{x-\xi}{(x-\xi)^2+d^2}p'^{(1)}(\xi)d\xi\right) \\ &\quad = -\omega^2 w^{(2)}(x) - 2i\omega U w'^{(2)}(x) + U^2 w''^{(2)}(x). \end{aligned} \quad (11b)$$

The first integral in Eq. (11) is treated as the Cauchy principal value. It is computed numerically using the Gauss-Chebyshev quadrature [15]. Due to the linearity of Eq. (11) in terms of the flag displacement, it is convenient to express the perturbation pressure in the form

$$p^{(j)}(x) = -\omega^2 p^{M(j)}(x) - 2i\omega U p^{G(j)}(x) + U^2 p^{K(j)}(x) \quad (12)$$

where the components with superscripts M, G and K correspond to added mass, gyroscopic effects and added stiffness, respectively [16].

Each pressure component is decomposed, using again the cantilever beam eigenfunctions, as follows:

$$\begin{aligned} p^{M(1)}(x) &= \sum_{n=1}^{Q}\alpha_n^M\psi_n(x), \quad p^{M(2)}(x) = \sum_{n=1}^{Q}\beta_n^M\psi_n(x), \\ p^{G(1)}(x) &= \sum_{n=1}^{Q}\alpha_n^G\psi_n(x), \quad p^{G(2)}(x) = \sum_{n=1}^{Q}\beta_n^G\psi_n(x), \\ p^{K(1)}(x) &= \sum_{n=1}^{Q}\alpha_n^K\psi_n(x), \quad p^{K(2)}(x) = \sum_{n=1}^{Q}\beta_n^K\psi_n(x). \end{aligned} \quad (13)$$

Inserting Eq. (13) into Eq. (11) lets the Cauchy principal values be computed with the known functions ψ_n, and the pressure coefficients can be solved in a simple system of equations. This procedure is different from the treatment in [12], in which a system of integral equations is solved with the unknown pressure components incorporated in the Cauchy principal values.

3.2 Flag displacements

Applying Galerkin method to Eq. (7a) yields

$$\begin{aligned} &\sum_{n=1}^{Q}\Big[\int_0^1 [A_n^{(1)}(\psi_n'''' - \omega^2\psi_n) \\ &\quad + (U^2\alpha_n^K - \omega^2\alpha_n^M - 2i\omega U\alpha_n^G)\psi_n]\psi_m dx \\ &\quad + A_n^{(1)}\mu U[i\omega\psi_n(1)\psi_m(1) - U\psi_n'(1)\psi_m(1)\Big] = 0 \end{aligned} \quad (14a)$$

and

$$\begin{aligned} &\sum_{n=1}^{Q}\Big[\int_0^1 [A_n^{(2)}(\psi_n'''' - \omega^2\psi_n) \\ &\quad + (U^2\beta_n^K - \omega^2\beta_n^M - 2i\omega U\beta_n^G)\psi_n]\psi_m dx \\ &\quad + A_n^{(2)}\mu U[i\omega\psi_n(1)\psi_m(1) - U\psi_n'(1)\psi_m(1)\Big] = 0 \end{aligned} \quad (14b)$$

for $m = 1, 2, 3, \ldots, Q$. Due to the orthogonality of the functions $\psi_n(x)$; i.e. $\int_0^1 \psi_n \psi_m dx = 0$ when $n \neq m$ and $= 1$ when $n = m$, the previous identities simplify to

$$\left(\begin{bmatrix} \mathbf{R} & \mathbf{0} \\ \mathbf{0} & \mathbf{R} \end{bmatrix} - \omega^2 \begin{bmatrix} \mathbf{I} & \mathbf{0} \\ \mathbf{0} & \mathbf{I} \end{bmatrix} + i\omega\mu U \begin{bmatrix} \mathbf{C} & \mathbf{0} \\ \mathbf{0} & \mathbf{C} \end{bmatrix} - \mu U^2 \begin{bmatrix} \mathbf{K} & \mathbf{0} \\ \mathbf{0} & \mathbf{K} \end{bmatrix} \right) \begin{pmatrix} \mathbf{A}_n^{(1)} \\ \mathbf{A}_n^{(2)} \end{pmatrix} - \omega^2 \begin{pmatrix} \mathbf{P}_1^M \\ \mathbf{P}_2^M \end{pmatrix} - 2i\omega U \begin{pmatrix} \mathbf{P}_1^G \\ \mathbf{P}_2^G \end{pmatrix} + U^2 \begin{pmatrix} \mathbf{P}_1^K \\ \mathbf{P}_2^K \end{pmatrix} = \begin{pmatrix} \mathbf{0} \\ \mathbf{0} \end{pmatrix}. \quad (15)$$

Above, $\mathbf{R}$ is a diagonal matrix with the nth diagonal entry $R_{nn} = r_n^4$, where r_n is the nth root of $1 + \cosh x \cos x = 0$; $\mathbf{I}$ is an identity matrix. The entries of $\mathbf{C}$ and $\mathbf{K}$ are $C_{mn} = \psi_m(1)\psi_n(1)$ and $K_{mn} = \psi'_m(1)\psi_n(1)$ with $m, n = 1, 2, \ldots, Q$. Quantities $\mathbf{P}_1$ and $\mathbf{P}_2$, with corresponding superscripts, are column vectors containing the pressure coefficients $\alpha_1, \ldots, \alpha_Q$ and $\beta_1, \ldots, \beta_Q$, obtained from the coefficients $\mathbf{A}_n^{(1)}$ and $\mathbf{A}_n^{(2)}$ by applying a Galerkin procedure to Eq. (11).

4. NUMERICAL RESULTS AND DISCUSSION

A convergence test is done first to test the accuracy of computation. It includes the number of terms (Q) in Eq. (10) and the number of quadrature points (N) for computing the Cauchy principal values in Eq. (11).

4.1 Convergence Test

A large enough number of Q in Eq. (10) is required for convergence of the eigenvalues. The first three eigenfrequencies are calculated for various Q as seen in Fig. 2. The eigenfrequencies converge rapidly, even with a few terms.

The Cauchy principal values in Eq. (11) have a general expression

$$f_n(x) = \int_0^1 \frac{\psi'_n(\xi)}{x - \xi} d\xi. \quad (16)$$

The lower beam mode shapes converge faster than the higher ones, and the highest mode shape is tested for convergence with increasing N on x, ξ, as shown in Fig. 3: $N = 200$ was found to be sufficient.

4.2 Onset of Instability

Solving Eq. (15) yields $4Q$ eigenfrequencies, and more specifically, $2Q$ conjugate pairs. One set of Q pairs corresponds to out-of-phase modes, and the other set, to in-phase modes. Therefore, only the eigenfrequencies with non-negative real parts are presented in this section.

Figures 4 and 5 are Argand diagrams of the first three dimensionless complex eigenfrequencies for $d = 1$ (large gap) and $d = 0.1$ (small relative gap). The real part indicates the frequency magnitude, and the imaginary part indicates damping. A negative imaginary part indicates that the corresponding mode is unstable. The numbers beside the dots are the values of dimensionless flow velocity. For $d = 1$ (Fig. 4), as the flow velocity is increased, the first eigenfrequency becomes purely imaginary and one of the solution branches crosses to the negative-plane, indicating the

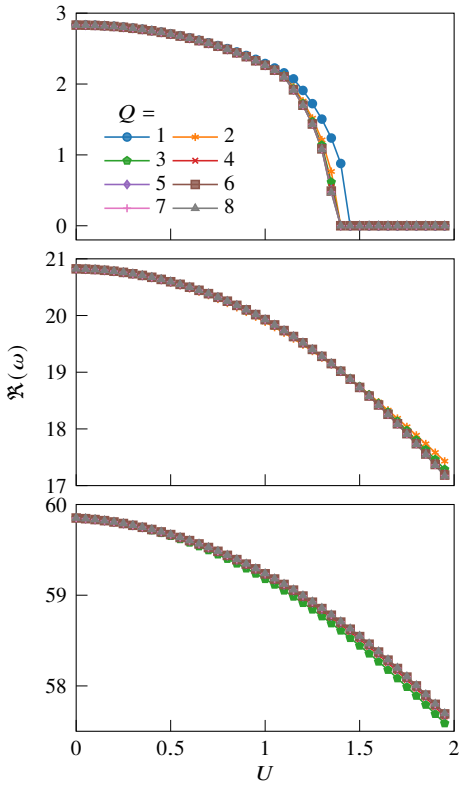

FIGURE 2: CONVERGENCE ANALYSIS ON EIGENFREQUENCIES: [TOP] FIRST, [MIDDLE] SECOND AND [BOTTOM] THIRD.

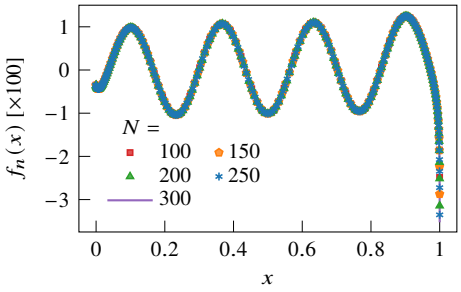

FIGURE 3: CONVERGENCE OF CAUCHY PRINCIPAL VALUES

onset of static divergence via a pitchfork bifurcation. When the instability occurs, the two flags will be out-of-phase. The second and third eigenfrequencies lose stability at higher flow velocities via Hopf bifurcations. The critical flow velocities for out-of-phase modes are lower than for in-phase modes.

For $d = 0.1$ (Fig. 5), the out-of-phase modes associated with the first two eigenfrequencies display different type of instability from the large gap. The first out-of-phase mode loses stability near zero flow velocity via flutter. Then as the flow velocity is increased, in-phase static divergence will occur. This critical flow velocity is lower than that for $d = 1$. For the second eigenfrequency, it is predicted that the in-phase mode loses stability at higher flow velocity via a Hopf bifurcation; however, the out-of-phase mode loses stability via static divergence, instead of flutter, at a very large flow velocity. Compared with the large gap, although the first mode in the small gap has a lower critical flow velocity, the

TABLE 1: CRITICAL FLOW VELOCITIES VERSUS d

d	0.01	0.02	0.03	0.04	0.05	0.06	0.07	0.08	0.09	
Flutter	0.002	0.004	0.005	0.007	0.009	0.012	0.014	0.017	0.020	
Divergence	0.526	0.775	0.974	1.138	1.272	1.381	1.436	1.450	1.450	
Flutter [12]	0.013	0.043	0.252							
Divergence [12]	1.431	1.431	1.431	1.432	1.432	1.432	1.432	1.433	1.433	
d	0.1	0.2	0.3	0.4	0.5	0.6	0.7	0.8	0.9	1
Flutter	0.023	0.106								
Divergence	1.451	1.453	1.456	1.458	1.461	1.463	1.465	1.467	1.469	1.471
Divergence [12]	1.433	1.435	1.436	1.438	1.439	1.440	1.440	1.441	1.442	1.442

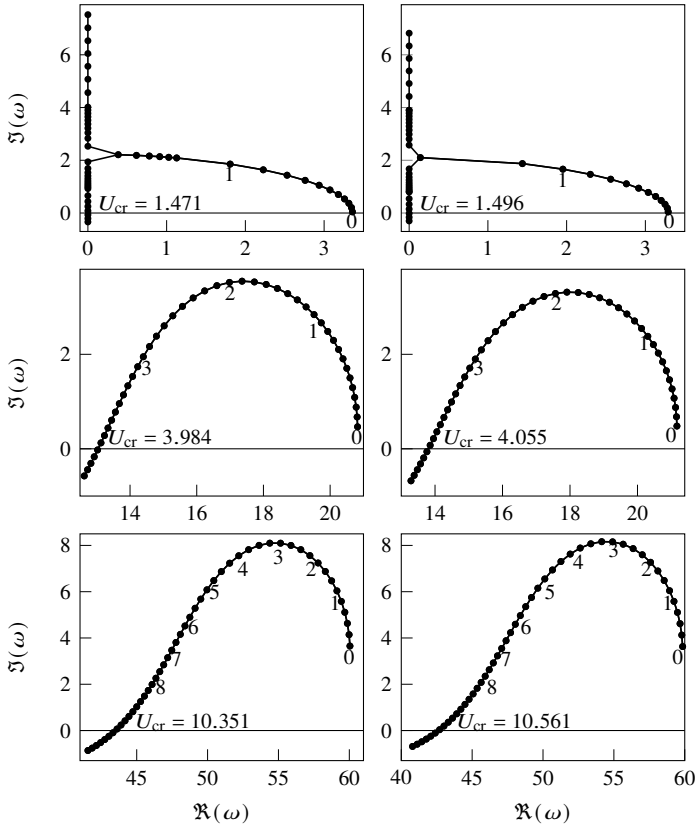

FIGURE 4: ARGAND DIAGRAMS FOR d = 1 FOR FIRST THREE EIGENFREQUENCIES: [TOP ROW] FIRST, [MIDDLE ROW] SECOND AND [BOTTOM ROW] THIRD; [LEFT COLUMN] OUT-OF-PHASE MODE, [RIGHT COLUMN] IN-PHASE MODE

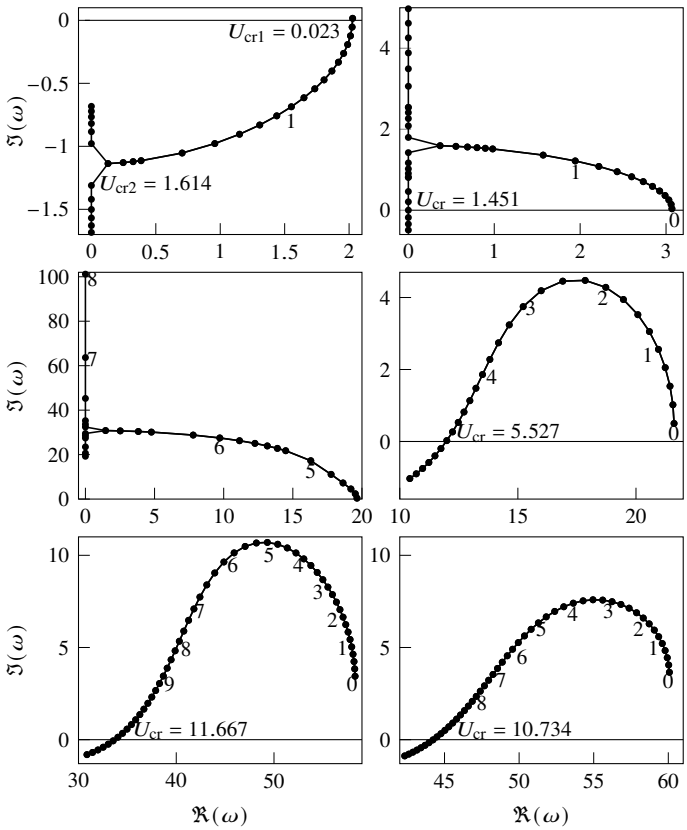

FIGURE 5: ARGAND DIAGRAMS FOR d = 0.1 FOR FIRST THREE EIGENFREQUENCIES: [TOP ROW] FIRST, [MIDDLE ROW] SECOND AND [BOTTOM ROW] THIRD; [LEFT COLUMN] OUT-OF-PHASE MODE, [RIGHT COLUMN] IN-PHASE MODE

higher modes have higher critical flow velocities.

The sensitivity of the critical flow velocity to d is listed in Table 1. Flutter occurs only for very small gaps. The critical flow velocity is near zero. As the gap is increased, only static divergence is present, and the critical flow velocity is slightly increased. The effect of d plays a role in Eq. (11). When d is smaller, the first and second integrals mathematically become less different. In other words, the perturbation pressure on one flag caused by the displacement of the other flag is naturally similar to the perturbation pressure caused by its own displacement, indicating strong coupling between the two flags. This could explain why the two flags lose stability at very low flow velocities.

5. CONCLUSION

The first three modes of two parallel inverted flags with varying gap in-between have been analyzed in this study. The perturbation pressure on a flag caused by its deflection is expressed by a Cauchy principal value in the model.

At a relatively large gap, out-of-phase or in-phase motions of the two flags are predicted, the former being dominant. The two flags are first subject to static divergence in the first mode, and the higher modes become unstable at higher flow velocities via Hopf bifurcations.

When the gap is reduced to a small value, the two flags first

show out-of-phase flutter in the first mode at a very low flow velocity and then have in-phase divergence at a high flow velocity. The in-phase motion becomes dominant in the higher modes. It can be predicted that when the gap $d \to 0$ the in-phase dominance makes the two flags act as a single flag.

ACKNOWLEDGEMENTS

The authors gratefully acknowledge the support of the Natural Sciences and Engineering Research Council of Canada.

REFERENCES

[1] Alam, Md. Mahbub, Chao, Li-Ming, Rehman, Shafiqur, Ji, Chunning and Wang, Hanfeng. "Energy harvesting from passive oscillation of inverted foil." *Physics of Fluids* Vol. 33 No. 7 (2021): p. 075111. DOI 10.1063/5.0056567.

[2] Kim, Daegyoum, Cossé, Julia, Huertas-Cerdeira, Cecilia and Gharib, Morteza. "Flapping dynamics of an inverted flag." *Journal of Fluid Mechanics* Vol. 736. DOI 10.1017/jfm.2013.555.

[3] Wang, Yan, Liu, Xiangyu, Chen, Tianyu, Wang, Hao, Zhu, Chuanqing, Yu, Hongyong, Song, Liguo, Pan, Xinxiang, Mi, Jianchun, Lee, Chengkuo and Xu, Minyi. "An underwater flag-like triboelectric nanogenerator for harvesting ocean current energy under extremely low velocity condition." *Nano Energy* Vol. 90 (2021): p. 106503. DOI 10.1016/j.nanoen.2021.106503.

[4] Rips, Aaron, Shoele, Kourosh and Mittal, Rajat. "Heat transfer enhancement in laminar flow heat exchangers due to flapping flags." *Physics of Fluids* Vol. 32 No. 6 (2020): p. 063603. DOI 10.1063/1.5142403.

[5] Huang, Lixi. "Flutter of cantilevered plates in axial flow." *Journal of Fluids and Structures* Vol. 9 No. 2 (1995): pp. 127–147. DOI 10.1006/jfls.1995.1007.

[6] Tavallaeinejad, Mohammad, Païdoussis, Michael, Legrand, Mathias and Kheiri, Mojtaba. "Instability and the post-critical behaviour of two-dimensional inverted flags in axial flow." *Journal of Fluid Mechanics* Vol. 890. DOI 10.1017/jfm.2020.111.

[7] Tavallaeinejad, Mohammad, Legrand, Mathias and Païdoussis, Michael. "Nonlinear dynamics of slender inverted flags in uniform steady flows." *Journal of Sound and Vibration* Vol. 467 (2020): p. 115048. DOI 10.1016/j.jsv.2019.115048.

[8] Sader, John, Cossé, Julia, Kim, Daegyoum, Fan, Boyu and Gharib, Morteza. "Large-amplitude flapping of an inverted flag in a uniform steady flow – a vortex-induced vibration." *Journal of Fluid Mechanics* Vol. 793 (2016): pp. 524–555. DOI 10.1017/jfm.2016.139.

[9] Goza, Andres, Colonius, Tim and Sader, John. "Global modes and nonlinear analysis of inverted-flag flapping." *Journal of Fluid Mechanics* Vol. 857 (2018): pp. 312–344. DOI 10.1017/jfm.2018.728.

[10] Tavallaeinejad, Mohammad, Païdoussis, Michael, Salinas, Manuel Flores, Legrand, Mathias, Kheiri, Mojtaba and Botez, Ruxandra. "Flapping of heavy inverted flags: a fluid-elastic instability." *Journal of Fluid Mechanics* Vol. 904. DOI 10.1017/jfm.2020.758.

[11] Rinaldi, Stephanie and Païdoussis, Michael. "Theory and experiments on the dynamics of a free-clamped cylinder in confined axial air-flow." *Journal of Fluids and Structures* Vol. 28 (2012): pp. 167–179. DOI 10.1016/j.jfluidstructs.2011.07.006.

[12] Michelin, Sébastien and Llewellyn Smith, Stefan. "Linear stability analysis of coupled parallel flexible plates in an axial flow." *Journal of Fluids and Structures* Vol. 25 No. 7 (2009): pp. 1136–1157. DOI 10.1016/j.jfluidstructs.2009.06.002.

[13] Guo, Changqing and Païdoussis, Michael. "Analysis of hydroelastic instabilities of rectangular parallel-plate assemblies." *Journal of Pressure Vessel Technology* Vol. 122 No. 4 (2000): pp. 502–508. DOI 10.1115/1.1286019.

[14] Eloy, Christophe, Souilliez, Claire and Schouveiler, Lionel. "Flutter of a rectangular plate." *Journal of Fluids and Structures* Vol. 23 No. 6 (2007): pp. 904–919. DOI 10.1016/j.jfluidstructs.2007.02.002.

[15] Erdogan, Fazil and Gupta, Ghanshyam. "On the numerical solution of singular integral equations." *Quarterly of Applied Mathematics* Vol. 29 No. 4 (1972): pp. 525–534. DOI 10.1090/qam/408277.

[16] Païdoussis, Michael. *Fluid-Structure Interactions: Slender Structures and Axial Flow*. Vol. 2. Academic Press (2004).